General Disclaimer

One or more of the Following Statements may affect this Document

- This document has been reproduced from the best copy furnished by the organizational source. It is being released in the interest of making available as much information as possible.

- This document may contain data, which exceeds the sheet parameters. It was furnished in this condition by the organizational source and is the best copy available.

- This document may contain tone-on-tone or color graphs, charts and/or pictures, which have been reproduced in black and white.

- This document is paginated as submitted by the original source.

- Portions of this document are not fully legible due to the historical nature of some of the material. However, it is the best reproduction available from the original submission.

X-660-77-21

PREPRINT

TMX 71269

BACKSCATTER OF HARD X-RAYS IN THE SOLAR ATMOSPHERE

T. BAI
R. RAMATY

JANUARY 1977

GSFC — GODDARD SPACE FLIGHT CENTER —
GREENBELT, MARYLAND

BACKSCATTER OF HARD X-RAYS IN THE SOLAR ATMOSPHERE

T. Bai* and R. Ramaty

Laboratory for High Energy Astrophysics

Goddard Space Flight Center

Greenbelt, Maryland 20771

*Also at the University of Maryland, College Park, Md.

Research Supported by NASA Grant 21-002-316.

ABSTRACT

The solar photosphere backscatters a substantial fraction of the hard X-rays from solar flares incident upon it. We have studied this reflection by using a Monte Carlo simulation which takes into account Compton scattering and photoelectric absorption. We have considered both isotropic and anisotropic X-ray sources, and we have evaluated the bremsstrahlung from an anisotropic distribution of electrons. We find that by taking the reflection into account, we can remove the inconsistency between recent observational data regarding the center-to-limb variation of solar X-ray emission and the predictions of models in which accelerated electrons are moving down toward the photosphere.

The backscattered photons create an observable albedo patch on the photosphere. If the height of the primary source is larger than its size, then the albedo patch can be distinguished from the primary source with detectors having high angular resolution. By resolving the albedo patch, information can be obtained on the ratio between the primary and reflected fluxes, on the scale size of the surface brightness of the patch, and, if the flare is not near the disk center, on the angular displacement of the primary source with respect to the centroid of the patch. Such data might become available from a detector on board NASA's Solar Maximum Mission (SMM), and could give information on the anisotropy and height of the primary X-ray source.

1. INTRODUCTION

Hard X-ray emission is a common phenomenon associated with solar flares. Photons in the energy range from 10 to 50 keV, when emitted down toward the photosphere, have a high probability of being reflected due to Compton scattering. This effect was first pointed out by Tomblin (1972), and was subsequently analyzed by Santangelo, Horstman and Horstman-Moretti (1973), and by Henoux (1975). As a result of this reflection, both the spectrum and the intensity of the X-rays are significantly modified, particularly for anisotropic X-ray sources which radiate predominantly in the downward direction. Furthermore, the reflection creates an albedo patch whose resolution from the primary X-ray source could give valuable information on the height of this source and on the anisotropy of the X-rays (Brown, van Beek and McClymont 1975).

In this paper we present a detailed treatment of X-ray reflection from the photosphere. We evaluate the spectrum and intensity of the sum of primary and reflected X-rays as a function of the flare location on the sun for isotropic and anisotropic X-ray sources. For isotropic sources we use both power-law and thermal X-ray spectra; for anisotropic sources we evaluate the bremsstrahlung of an anisotropic electron distribution. We also evaluate the surface brightness of the albedo patch resulting from the reflection by calculating the reflection probability as a function of the photon energy and its incident and reflected directions.

X-ray emission from electrons beamed down towards the photosphere has been treated by Brown (1972) and by Petrosian (1973). If reflection is ignored, X-ray emission from such electrons in the 10 to 50 keV region shows a large limb brightening which has not been detected by observations. By analyzing about 300 X-ray events observed by OGO-5, Kane (1974) reported that there was no center-to-limb variation in the frequency of X-ray events. Datlowe, Elcan, and Hudson (1974), who analyzed in detail 123 hard X-ray events observed by OSO-7 between 10 October 1971 and 6 June 1972, did not find any significant center-to-limb variations in X-ray fluxes, durations of the bursts, and frequencies of occurrences. Furthermore, these authors found that the spectra of limb flares are statistically slightly steeper than those of disk flares. As we shall show, this result, as well as the lack of limb brightening, is consistent with anisotropic X-ray emission with reflection taken into account.

If the size of the primary X-ray source is considerably smaller than its height, then in principle the primary source can be resolved from its albedo patch. When such resolution is possible, three independent measurements can give information on the height of the primary source and the anisotropy of the primary X-rays. These measurements are the ratio between the number of primary and reflected X-rays, the distribution of surface brightness of the albedo patch, and, if the primary source is not at the disk center, the displacement of the projection of the source with respect to the centroid of the albedo patch. Brown et al. (1975) have discussed the possibility of determining the height of

the primary X-ray source from the size of the albedo patch, and have shown that for small primary sources at heights ranging from about 10^3 to 5×10^4 km above the photosphere, such measurements could be performed by the Hard X-Ray Imaging Spectrometer that will be flown on NASA's Solar Maximum Mission. In their calculations, however, Brown et al. (1975) assumed that the reflection probability is independent of the incident direction of the photon. As we shall show, the reflection probability depends quite strongly on this direction; as a consequence, albedo patches from flares not close to the disk center are larger than found by these authors.

In Section 2 we describe the methods of the calculations, and in Section 3 we evaluate the reflection from isotropic X-ray sources. In Section 4 we calculate the X-ray emission, both direct and reflected, produced by accelerated electrons moving down toward the photosphere. In this section we also discuss the relationships of the center-to-limb variations of the fluxes and spectra of hard X-ray events to the anisotropy of the accelerated electrons, and compare the results with the data of Datlowe et al. (1974). In Section 5 we evaluate the reflection probabilities of monoenergetic and unidirectional photons. We then use these probabilities to calculate the surface brightness distribution of albedo patches from isotropic and anisotropic electrons, for two photon energies and two representative flare locations on the Sun. We summarize our results in Section 6.

2. METHODS OF CALCULATIONS

Hard X-rays released down to the photosphere are either Compton scattered or absorbed by the photoelectric effect. The differential Compton cross section is given by (Klein and Nishina 1929)

$$\frac{d\sigma_c}{d\Omega}(\epsilon_0, \theta_s) = \frac{1}{2} r_0^2 \left\{ \left(\frac{\epsilon}{\epsilon_0}\right)^3 + \frac{\epsilon}{\epsilon_0} - \left(\frac{\epsilon}{\epsilon_0}\right)^2 \sin^2 \theta_s \right\}. \quad (1)$$

Here θ_s is the scattering angle, $r_0 = 2.82 \times 10^{-13}$ cm, and ϵ_0 and ϵ are the initial and final photon energies related by

$$\epsilon = \epsilon_0 / [1 + (\epsilon_0/mc^2)(1 - \cos\theta_s)], \quad (2)$$

where mc^2 is the electron rest mass energy. The total Compton cross section is

$$\sigma_c(\epsilon_0) = 2\pi r_0^2 \left\{ \frac{1+\alpha}{\alpha^2} \left[\frac{2(1+\alpha)}{1+2\alpha} - \frac{\ln(1+2\alpha)}{\alpha} \right] + \frac{\ln(1+2\alpha)}{2\alpha} - \frac{1+3\alpha}{(1+2\alpha)^2} \right\}, \quad (3)$$

where $\alpha = \epsilon_0/mc^2$. In our calculation we multiply this cross section by 1.15 to take into account the effects of He and heavier elements.

We use the photoelectric absorption cross section, σ_a, given by Fireman (1974). At the energies of interest ($\gtrsim 10$ keV), this cross section depends mainly on the abundance of heavy elements such as O, Fe, and Ni. Fireman (1974) used the photospheric abundances given by Withbroe (1971). The following analytical form is a good approximation to the extrapolation of his result to energies $\gtrsim 10$ keV:

$$\sigma_a(\epsilon_0) = 7.2 \times 10^{-22} \epsilon_0^{-2.78} \ (\text{cm}^2/\text{H-atom}), \quad (4)$$

where ϵ_0 is in keV.

Throughout the present paper we assume that the photosphere is plane-stratified. We evaluate the backscattering of primary photons by using a Monte Carlo simulation. We generate photons distributed in accordance with a source function $Q(\epsilon_0, \theta_0, \varphi_0)$, where θ_0 and φ_0 are the polar and azimuthal angles of the photon in a system whose Z-axis is perpendicular to the photosphere. Photons with $\theta_0 < 90°$ move away from the Sun. If before the scattering the direction of the photon is defined by (θ_1, φ_1), then after the scattering the photon direction is given by (θ_2, φ_2), where

$$\cos\theta_2 = \cos\theta_1 \cos\theta_s - \sin\theta_1 \sin\theta_s \cos\varphi_s, \tag{5}$$

$$\cos\varphi_2 = (\cos\theta_1 \cos\varphi_1 \sin\theta_s \cos\varphi_s - \sin\varphi_1 \sin\theta_s \sin\varphi_s + \sin\theta_1 \cos\varphi_1 \cos\theta_s)/\sin\theta_2, \tag{6}$$

$$\sin\varphi_2 = (\cos\theta_1 \sin\varphi_1 \sin\theta_s \cos\varphi_s + \cos\varphi_1 \sin\theta_s \sin\varphi_s + \sin\theta_1 \sin\varphi_1 \cos\theta_s)/\sin\theta_2. \tag{7}$$

Here θ_s and φ_s are the polar and azimuthal angles of the scattered photon in a frame whose Z-axis is aligned with the direction of motion of the photon before the scattering.

We choose the initial energy of the photon, ϵ_0, such that photons are uniformly distributed in log ϵ_0 space, and we then take into account the energy spectrum of the primary X-rays by assigning each photon a weighted number proportional to its energy and the differential photon intensity at this energy. This procedure is more advantageous than the direct generation of photons with a desired energy spectrum for two reasons. First, in the latter procedure the

photon count statistics decreases rapidly with increasing energy, while with the present method the photon count statistics remains similar in each logarithmically spaced energy bin. Second, with the present method we can get the results corresponding to initial photons with various energy spectra with only one computer run by simply assigning the appropriate weighting factors to each photon.

We follow all the photons until they escape or are absorbed. The relationship between the energy of the photon before and after the scattering is given by equation (2), and the relationship between their directions of motion is given by equations (5) through (7). At each scattering, the angle θ_s is selected in accordance with the differential cross section given by equations (1) and (2), and φ_s is taken as a uniformly distributed random number. We collect the reflected photons according to their final energies, ϵ, and the directions of motion, (θ, φ), thereby defining a source function $Q'(\epsilon, \theta, \varphi)$.

From the above calculations we find that the escaping photons undergo on the average only a few scatterings. Since these scatterings take place at columnar depths of about 10^{24} cm^{-2}, photons are backscattered predominantly in the photosphere where the mean free path is of the order of 10^7 cm.

3. THE ALBEDO OF ISOTROPIC SOURCES

For the calculations of this section we use isotropic photon sources. We consider power-law sources given by

$$Q(\epsilon) = A\epsilon^{-s} \text{ (photons sr}^{-1}\text{ sec}^{-1}\text{ keV}^{-1}\text{)}, \qquad (8)$$

and optically thin thermal sources given by (e.g., Holt 1974)

$$Q(\epsilon) = 2.41 \times 10^{-16}\, g(T,\epsilon)\, Z^2\, n_e\, n_i\, V \times (kT)^{-3/2}\, (\epsilon/kT)^{-1} \exp(-\epsilon/kT) \left(\frac{\text{photons}}{\text{sr-sec-keV}}\right), \quad (9)$$

where ϵ and kT are in keV, Z is the atomic number of the medium, n_e and n_i are the electron and ion densities, V is the volume of the emitting source, and $g(T, \epsilon)$ is the Gaunt factor (Karzas and Latter 1961).

The differential reflectivity for such source is defined as

$$R(\epsilon,\theta,\varphi) = Q'(\epsilon,\theta,\varphi)/Q(\epsilon) \quad (10)$$

where Q' is the number of reflected photons in the direction (θ, φ) per (sr-sec-keV) due to the primary source $Q(\epsilon)$. The integral reflectivity is given by

$$\bar{R}(\epsilon) = (2\pi)^{-1} \int_0^{2\pi} d\varphi \int_0^1 d(\cos\theta)\, R(\epsilon,\theta,\varphi). \quad (11)$$

Figure 1 shows the integral reflectivities of isotropic sources with power-law and thermal spectra. As can be seen, the reflectivity is maximum around 30 keV. At lower energies the reflectivity is reduced by photoelectric absorption, and at higher energies the reflectivity decreases because in the scattering process photons emerge preferentially in the forward direction. Furthermore, because higher energy photons lose energy in Compton scattering, the reflectivity at high energies is larger for flatter photon spectra.

The properties of the differential reflectivity are investigated in Figure 2, which shows the quantity $1 + R(\epsilon, \theta)$ for various values of the direction of observation, θ, and two incident photon spectra. As can be seen, below ~250 keV the reflectivity is larger at smaller values of θ, because the amount of matter traversed by the reflected photon is smaller in these cases. This trend is reversed

at higher energies, because at these energies the cross section for large angle scattering is small.

The idea that solar hard X-rays are produced by hot thermal electrons began to gather new interest recently (Colgate, Audouze and Fowler 1977). In Figure 3 we show the total (primary and reflected) photon spectrum of thermal X-ray sources for kT = 20 and 30 keV and two directions of observation. As can be seen, even though the total spectra are somewhat steeper than the primary spectra, they cannot be well approximated by single power laws.

4. ANISOTROPIC SOURCES

For the calculations of this section, we assume that X-rays are produced by accelerated electrons with momentum vectors uniformly distributed in a cone of 30° half opening angle centered around the downward vertical vector. The distribution function of the momentum vectors of such electrons is

$$g(\theta') = \begin{cases} 1/[2\pi(1-\cos 30°)] & \text{for } 150° \leq \theta' \leq 180° \\ 0 & \text{otherwise,} \end{cases} \tag{12}$$

where θ' is the polar angle measured from the normal to the plane-stratified photosphere. We also assume that the instantaneous electron energy spectra are power laws with power-indexes 2.5 and 3.5.

The bremsstrahlung produced by these electrons leads to a photon source given by

$$Q(\epsilon,\theta) = n \int d\Omega'' \int_{\epsilon}^{\infty} dE\, N(E)\, g'(\theta'',\varphi'')\, v(E)\, \frac{d^2\sigma(E,\epsilon,\theta'')}{d\epsilon\, d\Omega''}. \tag{13}$$

Here N(E) is the instantaneous differential electron number, n is the ambient density, v(E) is the electron velocity, θ is the angle between the line of sight and the normal to the photosphere, θ'' is the polar angle of the electron momentum vector measured from the line of sight, $\frac{d^2\sigma}{d\epsilon\, d\Omega''}$ (E, ϵ, θ'') is the differential bremsstrahlung cross-section, and $g'(\theta'', \varphi'')$ is the angular distribution function of the velocity vectors of the electrons in the coordinate system whose Z-axis is the line of sight.

Using the above equation and the Formula 2BN in Koch and Motz (1959) for the differential cross section (non-screened), we calculate the X-ray production rate, $Q(\epsilon, \theta)$, for various values of ϵ and θ. The results are shown by solid lines in Figures 4 and 5 for electron distributions with power indexes 2.5 and 3.5, respectively. In this figure, 90° corresponds to X-ray emission from the solar limb, and 0° to emission at the disk center. Without the reflection of the X-rays, there would be a large limb brightening and a slight limb flattening of the photon spectra. Similar results were obtained by Brown (1972) and by Petrosian (1973). The dashed lines in these figures show the resultant total photon production rates including the primary and reflected sources. As can be seen, the limb brightening effect has almost disappeared except at very low energies or at very high energies where the reflectivity is small (Figure 1). Henoux (1975) also reported similar results. Therefore, the anisotropic model in which electrons are moving toward the photosphere is not contradictory to the results of Datlowe et al. (1974, 1976) when the reflected component is properly taken into account.

Figure 6 shows the photon spectra due to anisotropic sources, taken from Figures 4 and 5 for several observation angles. Even though over the entire energy range the photon spectra deviate from power laws, in the 15 to 50 keV they can be reasonably well approximated by a single power law. The resultant spectral indexes for this energy range are shown in Table 1. Similar approximations can be made for the isotropic power-law and themal sources. As can be seen, for the isotropic sources, the spectral index does not change appreciably with heliocentric angle because reflection is not the dominant source of photons in this case. On the other hand, for the anisotropic sources the photon spectrum steepens as the heliocentric angle increases, a fact that can account for the result of Datlowe et al. (1974) who found that the average spectral index (in the 17 to 45 keV range) of limb flares is larger by about 0.5 than of disk flares.

One of the characteristics of the spectra shown in Figure 6 is that for flares near the disk center the spectra steepen as energy increases, but this character is less pronounced for limb flares. Therefore, if the accelerated electrons in flares are beamed downward, the spectra measured at energies $\gtrsim 100$ keV will show a limb flattening in contrast to the spectra measured at energies $\lesssim 50$ keV. This may be tested in future experiments. If the steepening of the spectrum at energies $\gtrsim 100$ keV is larger for flares near the disk center than for flares near the limb, it can be regarded as a supporting evidence for the anisotropic model.

5. THE ALBEDO PATCH

In this section we calculate the distribution of surface brightness of the albedo patch for X-ray emission from a primary point source. We define $P(\epsilon_0, \theta_0, \theta, \varphi)$ as the probability for a photon with energy ϵ_0 incident upon the photosphere with polar angle θ_0 to be reflected per unit solid angle along the direction (θ, φ), where φ is the angle between the projections on the photosphere of the incident and reflected directions. Here we normalize P such that the integral of P over θ and φ is 1 when there is no absorption. In order to calculate this probability we use the Monte Carlo simulation described in Section 2. The results are shown in Figures 7 and 8 for $\epsilon_0 = 30\,\text{keV}$ and $\epsilon_0 = 15\,\text{keV}$, respectively. The probability of reflection for $\theta = 0°$ (not shown in these figures) is almost constant equal to about 0.8 for $\epsilon_0 = 30\,\text{keV}$ and about 0.3 for $\epsilon_0 = 15\,\text{keV}$. For larger values of θ, however, P is not a constant.

The value of P is determined by the combined effects of the angular dependence of the Compton scattering cross section and the probability for escape determined by the amount of material traversed before and after the scattering process. For example, for a given observation angle θ, P increases as θ_0 decreases from vertical incidence ($\theta_0 = 180°$), mainly because less material is traversed by the escaping photons when θ_0 is small than when θ_0 is large. For the same reason, the variation with θ_0 is steeper for 15 keV than for 30 keV, because absorption is more important at lower energies. On the other hand, for a given θ_0 ($>90°$), P decreases as θ increases from $\theta = 0°$ (vertical escape)

because also in this case increasingly larger amounts of material are traversed by the escaping photons. The dependence of P on φ is due mainly to the angular dependence of the Compton cross section.

As we have mentioned earlier, for $\theta \simeq 0°$, P is almost independent of θ_0 and of course it does not depend on φ. This effect is caused by the fact that as θ_0 decreases from 180° both the Compton cross section and the amount of material traversed by the escaping photons decrease and these two decreases have opposite effects on the reflection probability. Furthermore, because of this effect, the variation of P with θ_0 is less steep when θ is small than when θ is large. Note that for $\theta = 0°$ and $\theta_0 = 180°$ we have backward scattering for which the Compton cross section is maximal in the nonrelativistic region.

In the calculations of Brown et al. (1975), it was assumed that the reflection probability is constant. From the above discussion it follows that this assumption is valid only for flares near the disk center. The net effect of the increase of P with decreasing θ_0 (Figures 7 and 8) is to make the albedo patch larger than the patch which would be obtained by using a constant P.

The surface brightness of the albedo patch (measured in photons sr^{-1} cm^{-2} sec^{-1}) observed at an angle θ due to a point source of monoenergetic photons incident on the photosphere is proportional to the number of photons incident upon unit area and their probability of reflection:

$$I(\theta,\ell,\varphi) = \Gamma(\theta_0,\varphi)\,[h^2\,\{(\ell/h)^2+1\}^{3/2}]^{-1}\;P(\epsilon_0,\theta_0,\theta,\varphi)\;. \qquad (14)$$

Here $f(\theta_0, \varphi)$ represents the number of photons (measured in sr^{-1} sec^{-1}) incident along the direction (θ_0, φ), h is the height of the source, and $\ell = -h \tan \theta_0$. Equation (14) implicitly assumes that the photon enters and escapes from the photosphere at the same position. This assumption is generally valid because the height of the X-ray source is believed to be much larger than the mean free path of the photon in the photosphere, which is only about 10^7 cm.

Equation (14) gives the surface brightness due to a mono-energetic primary source. As we have seen in Section 3, the reflectivity (which is proportional to the integral of I over ℓ and φ) does depend on the spectrum of the primary source. However, because the energy loss during the scattering process in the energy range from about 10 to 30 keV is not large (about 4 keV at $\epsilon_0 = 30$ keV and about 1 keV for $\epsilon_0 = 15$ keV), the angular dependence of P and I are not strongly dependent on the primary spectrum. Therefore, we plot the isobrightness contours of the albedo patch by using equation (14).

The results are shown in Figure 9 for various cases, where the scale is given in units of the height of the source, h. By comparing cases a and b, we see that the albedo patches are larger for larger values of θ. This result is a direct consequence of behavior of P as shown in Figure 7. Furthermore, by comparing cases b and c we see that the size of the albedo patch decreases with increasing energy, and this result is also a consequence of the behavior of P as can be seen by comparing Figures 7 and 8. Finally, by comparing cases a and d, we see that the albedo patch becomes smaller for the anisotropic case than

for the isotropic case. However, since at energies below about 20 keV X-ray emission in the forward hemisphere is almost independent of observation angle (Figures 4 and 5), the size of the albedo patch at these energies is essentially independent of the anisotropy of the primary X-ray source.

6. SUMMARY AND CONCLUSION

The reflectivity of hard X-rays depends on the energy and the spectral shape of the primary photons. The reflectivity is largest for flares near the disk center, for flat photon spectra and for photon energies around 35 keV. For example, for an isotropic source at the disk center with differential number spectrum ϵ^{-3}, the ratio between the reflected and primary fluxes is about 0.8 at maximum value. As a result of the reflection, for isotropic sources with power-law spectra the X-ray spectrum in the 15 to 50 keV range becomes slightly flatter than the primary spectrum. As can be seen from Table 1, this flattening is essentially independent of the position of the flare on the Sun.

For X-rays produced by electrons moving toward the photosphere there is no strong variation of the brightness of the X-ray emission with position of the flare on the Sun in the 15 to 50 keV range (Figures 4 and 5). This result is quite different from the large center-to-limb variation that would be obtained from such electrons if reflection were not taken into account. The X-ray spectrum from such electrons steepens significantly as the position of the flare moves from the disk center to the limb. Such limb steepening is a unique consequence of reflection, and together with the lack of limb brightening, is consistent with data on the

center-to-limb variation of solar X-ray emission (Kane 1974, Datlowe et al. 1974, 1976). At higher energies (>100 keV), however, the backscatter is negligible and therefore X-ray emission from downward moving electrons should show a strong limb brightening and limb flattening.

Provided that the primary X-ray source can be resolved from its albedo patch, the ratio between primary and reflected photon fluxes, the size of the albedo patch, and the displacement of the primary X-ray source from the centroid of the patch, can give information on the anisotropy and height of X-ray source.

REFERENCES

Brown, J. C.: 1972, Solar Phys. 26, 441.

Brown, J. C., van Beek, H. F., and McClymont, A. N.: 1975, Astron. Astrophys. 41, 395.

Colgate, S. A., Audouze, J., and Fowler, W. A.: 1977, to be published.

Datlowe, D. W., Elcan, M. J., and Hudson, H. S.: 1974, Solar Phys. 39, 155.

Datlowe, D. W., Elcan, M. J., and Hudson, H. S.: 1977, to be published.

Fireman, E. L.: 1974, Ap. J. 187, 57.

Henoux, J. C.: 1975, Solar Phys. 42, 219.

Holt, S. S.: 1974; in High Energy Quanta in Astrophysics, edited by McDonald and Fichtel, MIT Press, p. 312.

Kane, S. R.: 1974, in G. Newkirk, Jr. (ed.), Coronal Disturbances, IAU Symp. 57, 105.

Karzas, W. J. and Latter, R.: 1961, Ap. J. Suppl. 6, 167.

Klein, O. and Nishina, Y.: 1929, Z. Physik. 52, 853.

Koch, H. W. and Motz, J. W.: 1959, Rev. Modern Phys. 31, 920.

Petrosian, V.: 1973, Ap. J. 186, 291.

Santangelo, N., Horstman, H., and Horstman-Moretti, E.: 1973, Solar Phys. 29, 143.

Tomblin, F. F.: 1972, Ap. J. 171, 377.

Withbroe, G. L.: 1971, in The Menzel Symposium, NBS Special Pub. 353, ed. K. B. Gebbie (Washington: U.S. G.P.O.), p. 127.

Table 1

Spectral Indexes of Photon Spectra in the Range from 15 keV to 50 keV

(a) Isotropic Photon Sources with Power-law Spectra

Original Photon Spectral Index	θ 5°	45°	75°
2	1.76	1.78	1.88
3	2.85	2.88	2.95
4	3.94	3.94	3.95
5	4.97	4.97	4.98

(b) Anisotropic Sources

Spectral Index of the Electrons	θ 5°		45°		75°	
	No Reflection	Reflection	No Reflection	Reflection	No Reflection	Reflection
^.5	3.48	2.68	3.52	2.80	3.40	3.06
3.5	4.44	3.81	4.49	3.96	4.39	4.12

FIGURE CAPTIONS

Figure 1. Integral reflectivities of isotropic X-ray sources. The reflectivity is defined in equations 10 and 11.

Figure 2. $1 + R(\epsilon, \theta)$ for isotropic sources with power-law spectra, where $R(\epsilon, \theta)$ is the differential reflectivity defined in equation 10.

Figure 3. Photon spectra due to a thermal hydrogen plasma with $n_e = n_i = 1\,cm^{-3}$, and $kT = 20\,keV$ and $kT = 30\,keV$. The resultant spectra (including the reflected component) seen at $\theta = 5°$ and at $\theta = 75°$ are shown by the solid lines. The dashed lines indicate the original spectrum.

Figure 4. Photon intensities due to the accelerated electrons moving toward the photosphere with velocity vectors uniformly distributed in a cone with half opening angle 30° and centered at the vertical to the photosphere. The spectrum of the accelerated electrons is $E^{-2.5}$. The solid lines represent primary photon intensities and the dashed lines represent the sum of the primary and reflected photons.

Figure 5. Same as Figure 4, except that the electron spectrum is $E^{-3.5}$.

Figure 6. Photon spectra taken from the results of Figures 4 and 5; θ is the angle between the direction of observation and the normal to the photosphere.

Figure 7. Reflection probabilities as functions of the direction of observation and the direction of the incident photon for photon energies of 30 keV; θ and θ_0 are the angles between the vertical to the photosphere and

FIGURE CAPTIONS

Figure 1. Integral reflectivities of isotropic X-ray sources. The reflectivity is defined in equations 10 and 11.

Figure 2. $1 + R(\epsilon, \theta)$ for isotropic sources with power-law spectra, where $R(\epsilon, \theta)$ is the differential reflectivity defined in equation 10.

Figure 3. Photon spectra due to a thermal hydrogen plasma with $n_e = n_i = 1\,cm^{-3}$, and $kT = 20\,keV$ and $kT = 30\,keV$. The resultant spectra (including the reflected component) seen at $\theta = 5°$ and at $\theta = 75°$ are shown by the solid lines. The dashed lines indicate the original spectrum.

Figure 4. Photon intensities due to the accelerated electrons moving toward the photosphere with velocity vectors uniformly distributed in a cone with half opening angle 30° and centered at the vertical to the photosphere. The spectrum of the accelerated electrons is $E^{-2.5}$. The solid lines represent primary photon intensities and the dashed lines represent the sum of the primary and reflected photons.

Figure 5. Same as Figure 4, except that the electron spectrum is $E^{-3.5}$.

Figure 6. Photon spectra taken from the results of Figures 4 and 5; θ is the angle between the direction of observation and the normal to the photosphere.

Figure 7. Reflection probabilities as functions of the direction of observation and the direction of the incident photon for photon energies of 30 keV; θ and θ_0 are the angles between the vertical to the photosphere and

the direction of observation and the direction of the incident photon, respectively; φ is the angle between the projection of these two directions on the photosphere.

Figure 8. Same as Figure 7, except that the incident photons are at 15 keV.

Figure 9. Isobrightness contours of the albedo patch for various cases. Starting from the center brightness drops by a factor 2 from one contour to the next.

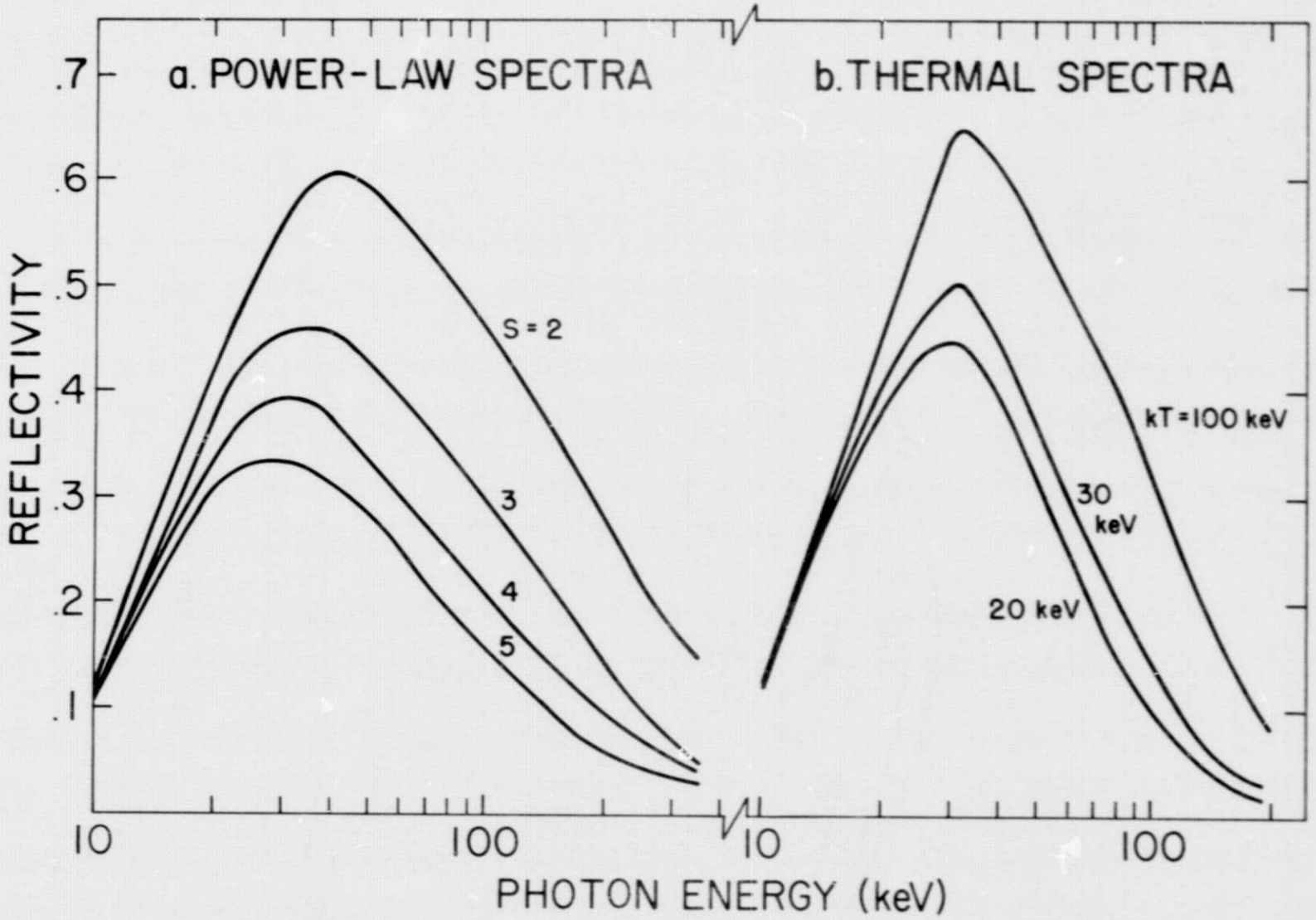
a. POWER-LAW SPECTRA
b. THERMAL SPECTRA
REFLECTIVITY
.7
.6
.5
.4
.3
.2
.1
S = 2
3
4
5
kT = 100 keV
30 keV
20 keV
10
100
10
100
PHOTON ENERGY (keV)

Fig. 1

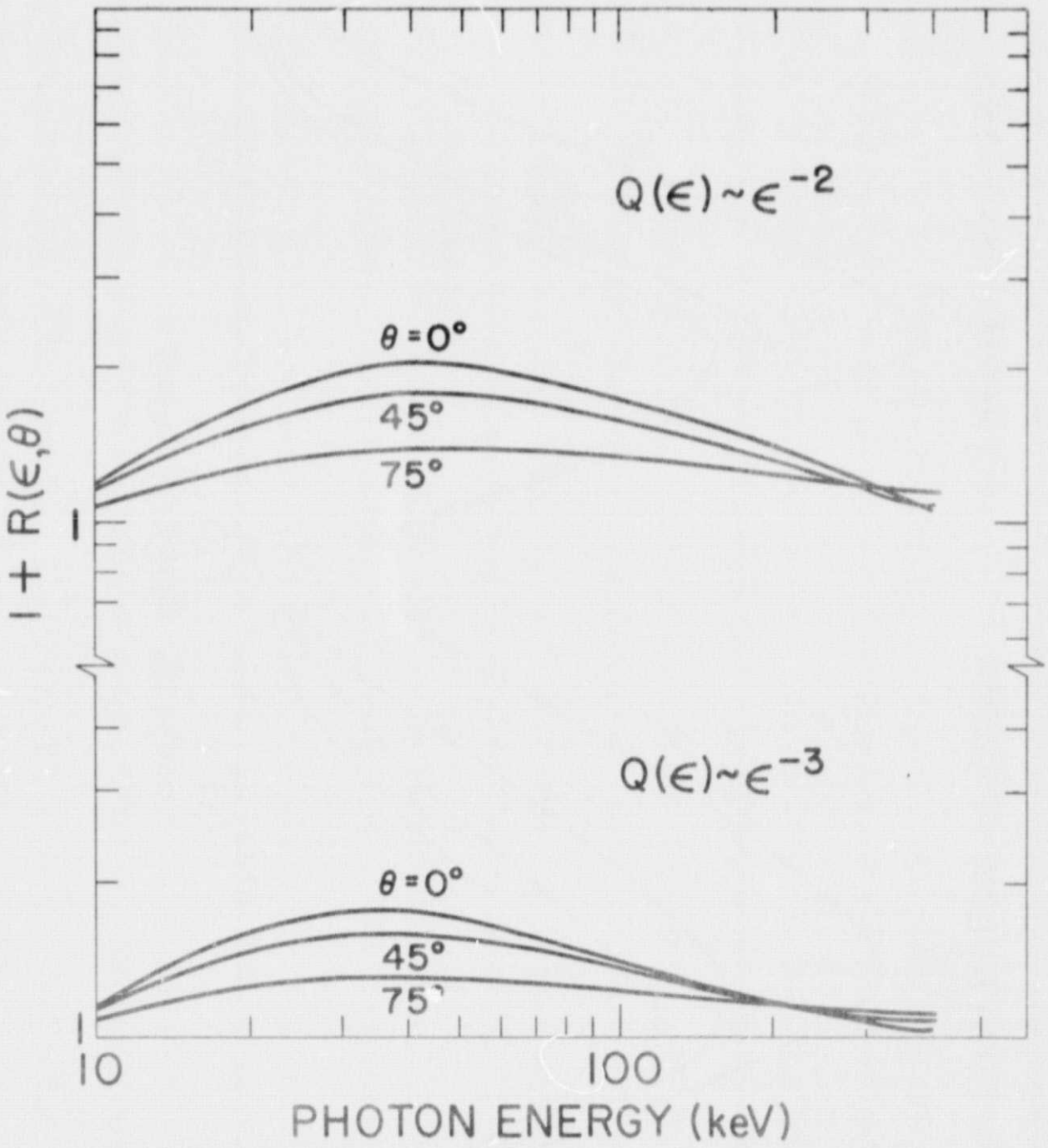
$Q(\epsilon)\sim\epsilon^{-2}$
$\theta=0°$
45°
75°
$1+R(\epsilon,\theta)$
1
$Q(\epsilon)\sim\epsilon^{-3}$
$\theta=0°$
45°
75°
1
10
100
PHOTON ENERGY (keV)

Fig. 2

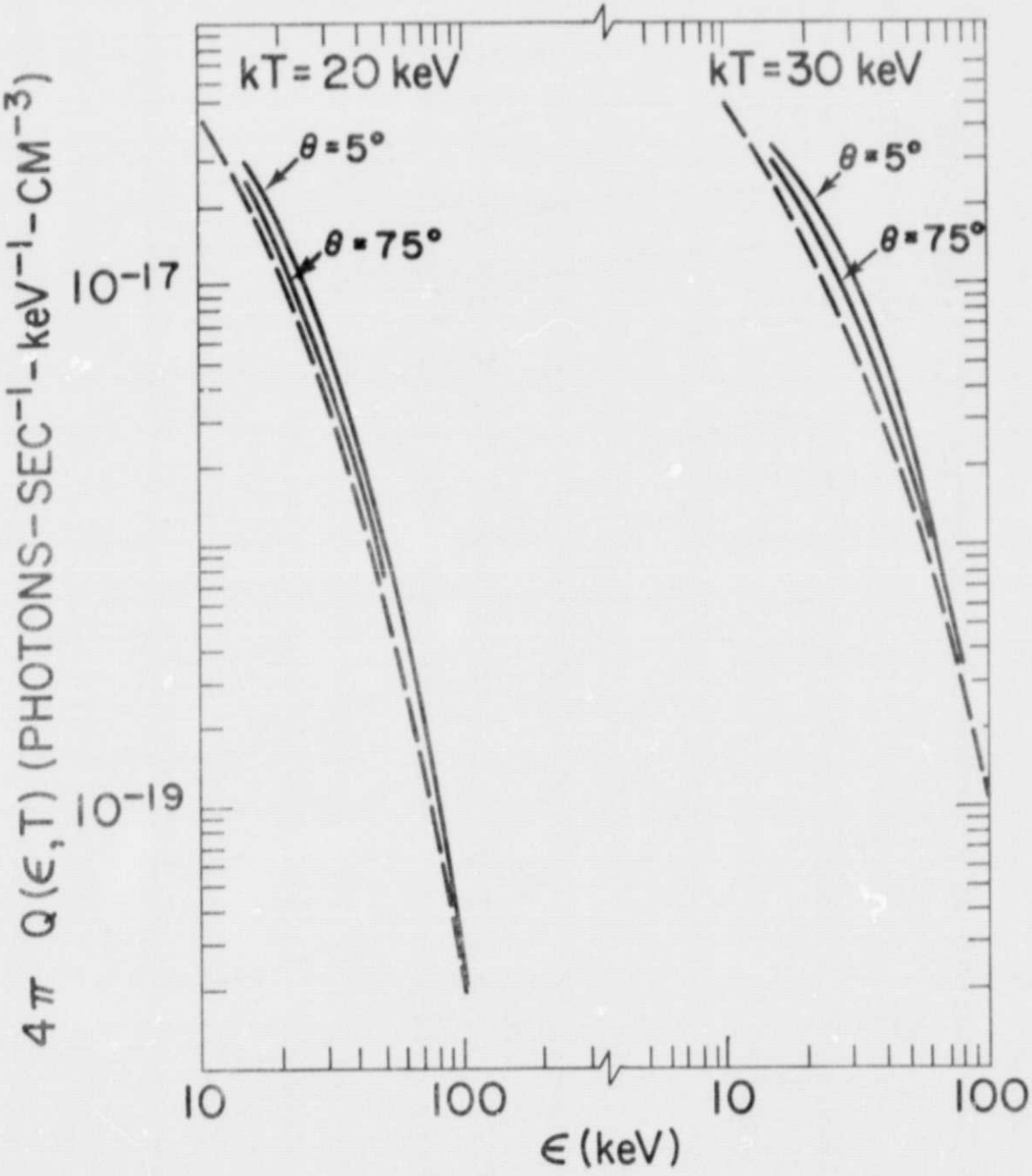
kT = 20 keV
kT = 30 keV
θ = 5°
θ = 75°
θ = 5°
θ = 75°
10⁻¹⁷
10⁻¹⁹
4π Q(ϵ, T) (PHOTONS-SEC⁻¹-keV⁻¹-CM⁻³)
10
100
10
100
ϵ (keV)

Fig. 3

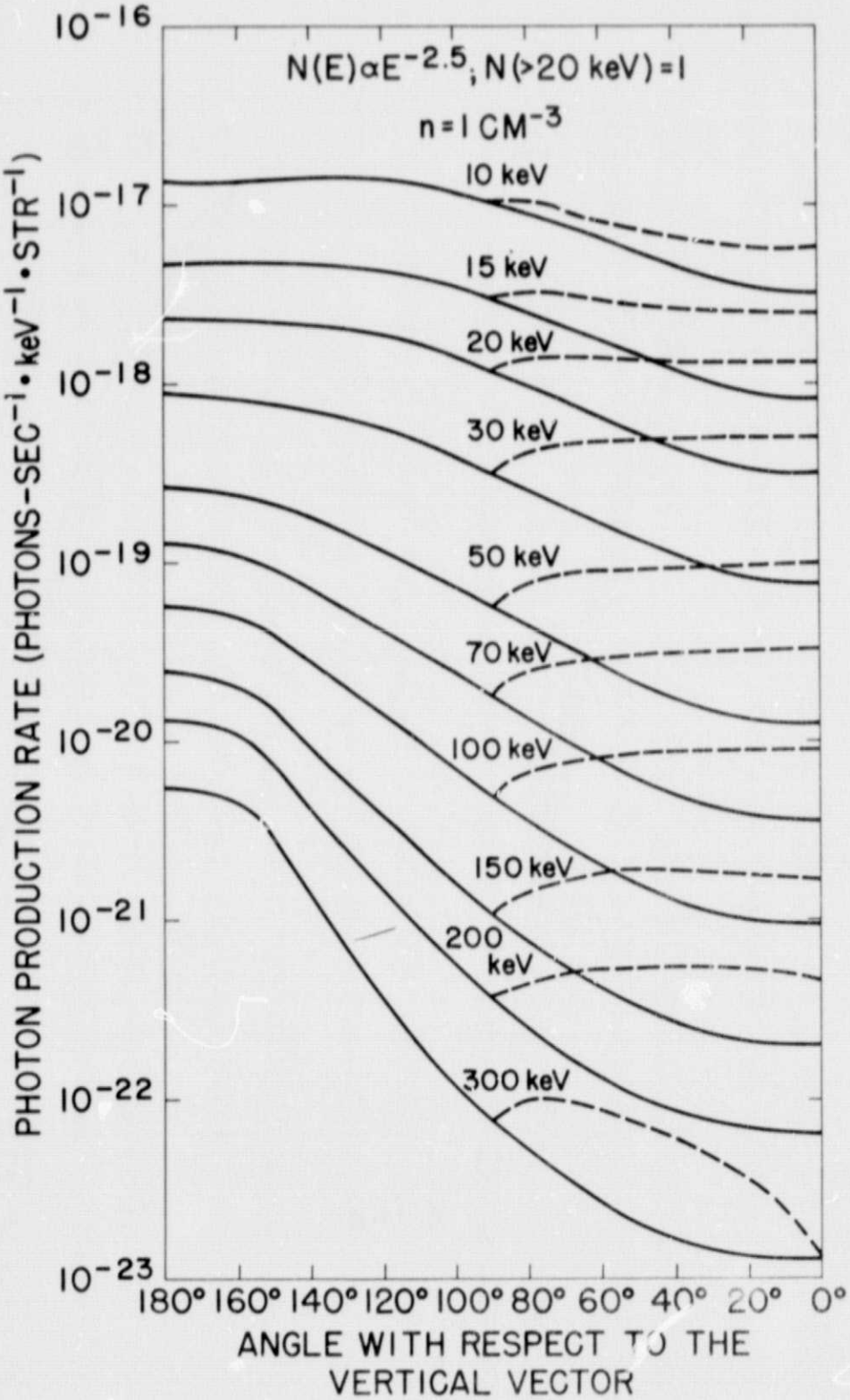
$N(E) \alpha E^{-2.5}$; $N(>20\ keV) = 1$
$n = 1\ CM^{-3}$
10 keV
15 keV
20 keV
30 keV
50 keV
70 keV
100 keV
150 keV
200 keV
300 keV
10^{-16}
10^{-17}
10^{-18}
10^{-19}
10^{-20}
10^{-21}
10^{-22}
10^{-23}
PHOTON PRODUCTION RATE (PHOTONS-SEC^{-1} • keV^{-1} • STR^{-1})
180° 160° 140° 120° 100° 80° 60° 40° 20° 0°
ANGLE WITH RESPECT TO THE VERTICAL VECTOR

Fig. 4

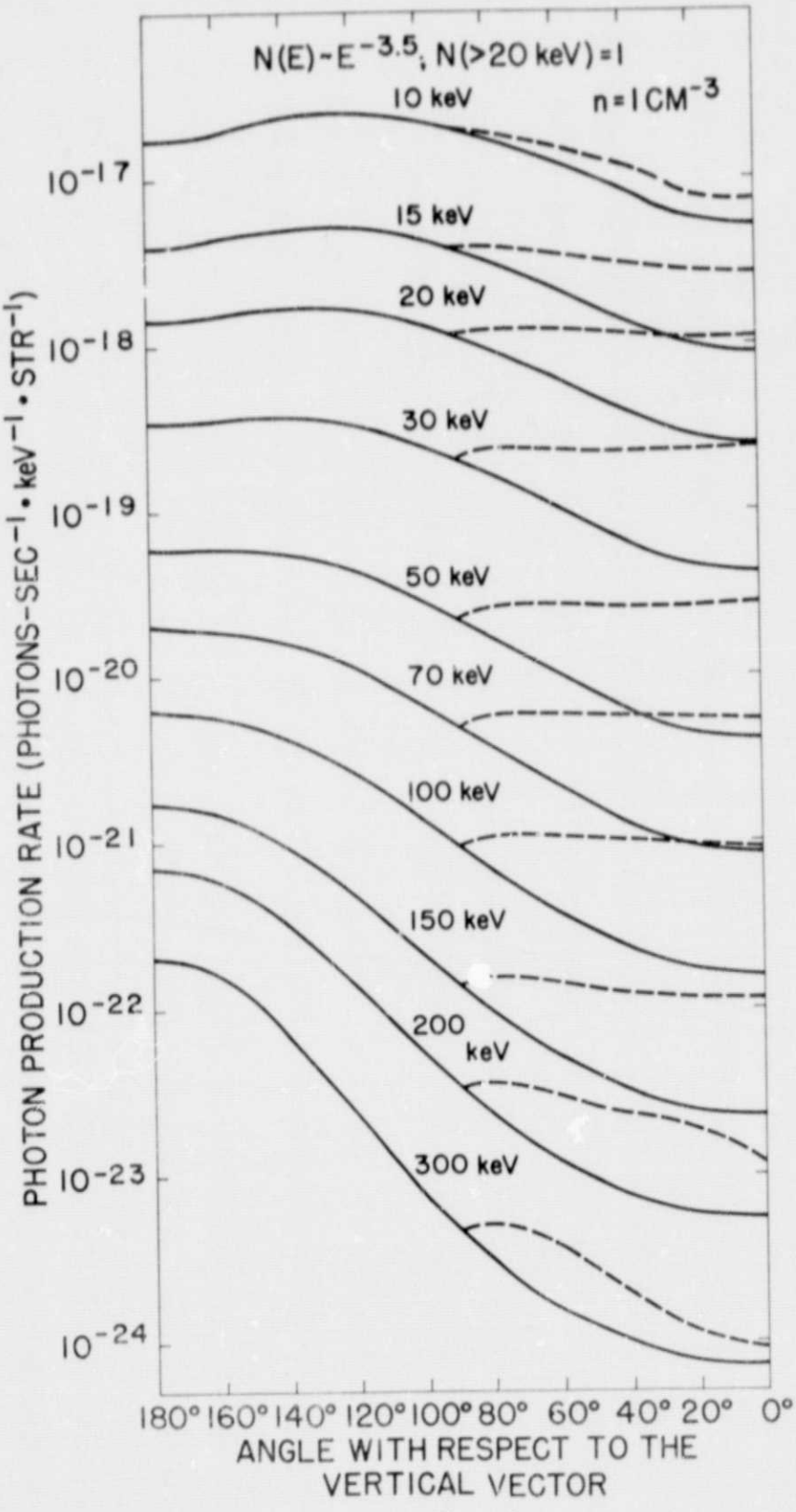
N(E)~E^-3.5; N(>20 keV)=1
n=1 CM^-3
10 keV
15 keV
20 keV
30 keV
50 keV
70 keV
100 keV
150 keV
200 keV
300 keV
10^-17
10^-18
10^-19
10^-20
10^-21
10^-22
10^-23
10^-24
PHOTON PRODUCTION RATE (PHOTONS-SEC^-1 • keV^-1 • STR^-1)
180° 160° 140° 120° 100° 80° 60° 40° 20° 0°
ANGLE WITH RESPECT TO THE VERTICAL VECTOR

Fig. 5

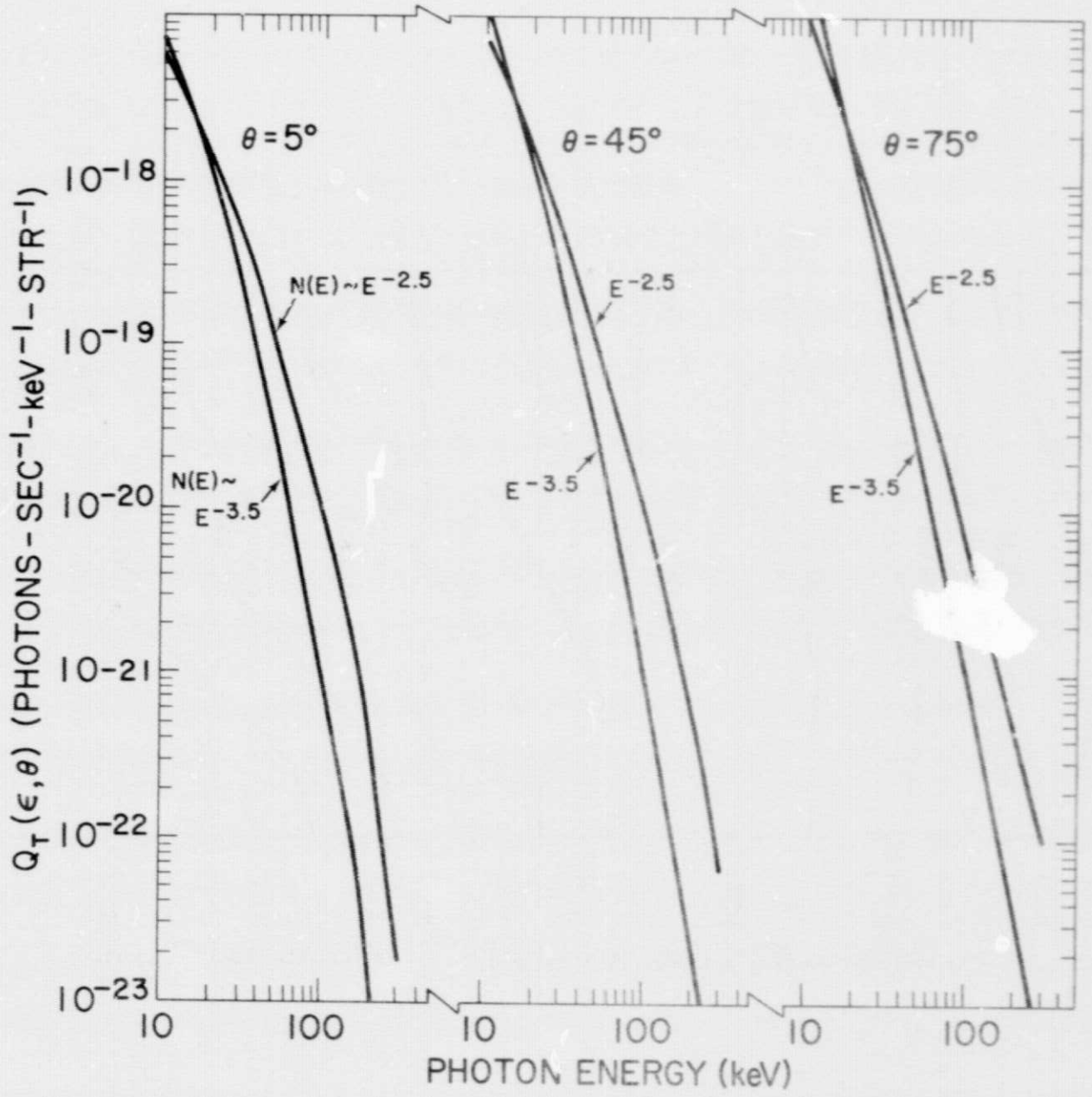
θ=5°
θ=45°
θ=75°
N(E)~E^-2.5
N(E)~ E^-3.5
E^-2.5
E^-3.5
E^-2.5
E^-3.5
Q_T(ε,θ) (PHOTONS-SEC^-1-keV^-1-STR^-1)
10^-18
10^-19
10^-20
10-21
10^-22
10^-23
10
100
10
100
10
100
PHOTON ENERGY (keV)

Fig.6

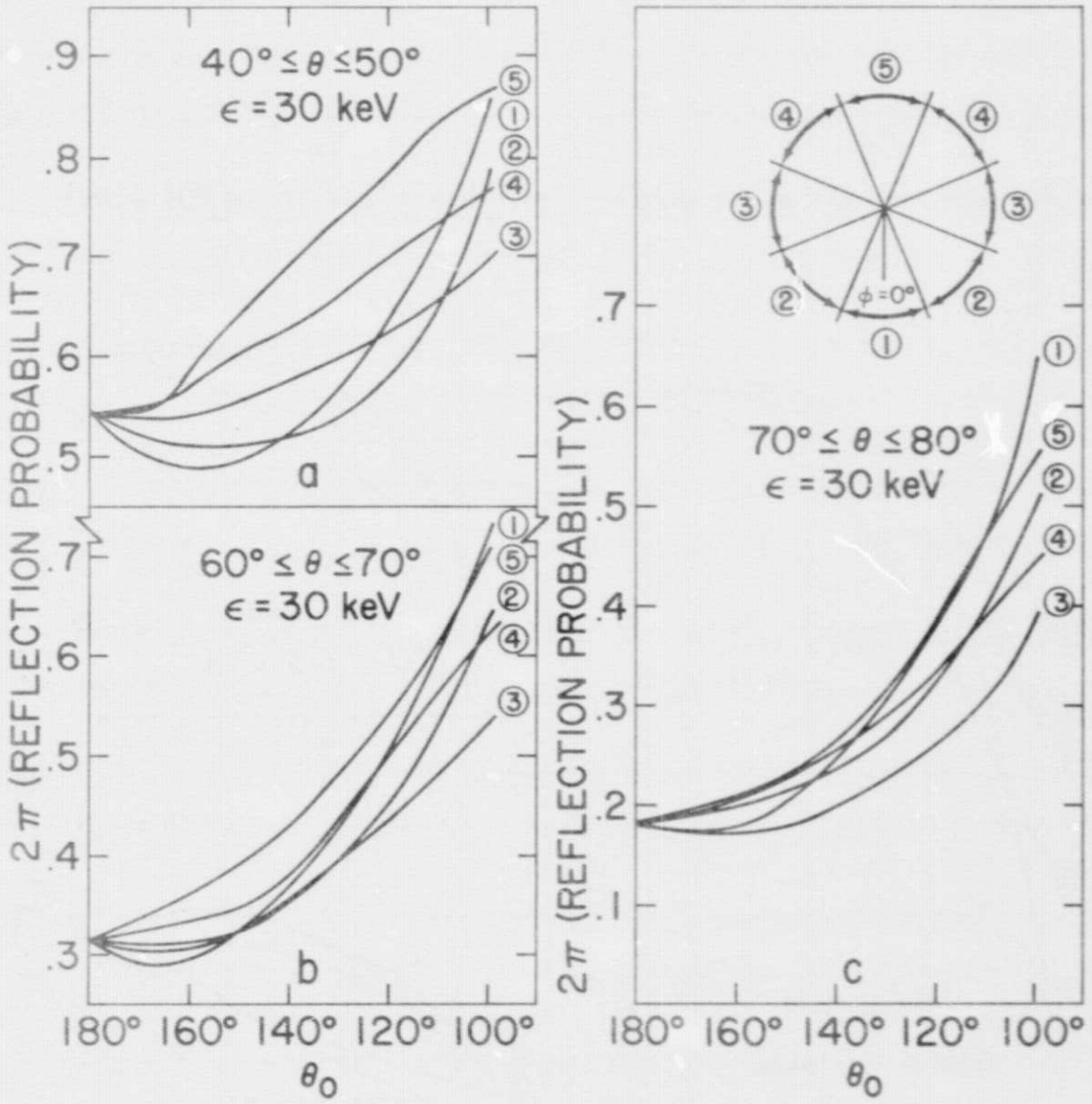
40° ≤ θ ≤ 50°
ϵ = 30 keV
a
60° ≤ θ ≤ 70°
ϵ = 30 keV
b
70° ≤ θ ≤ 80°
ϵ = 30 keV
c
2π (REFLECTION PROBABILITY)
θ0
180° 160° 140° 120° 100°
.9 .8 .7 .6 .5 .4 .3 .2 .1
ϕ = 0°
① ② ③ ④ ⑤

Fig. 7

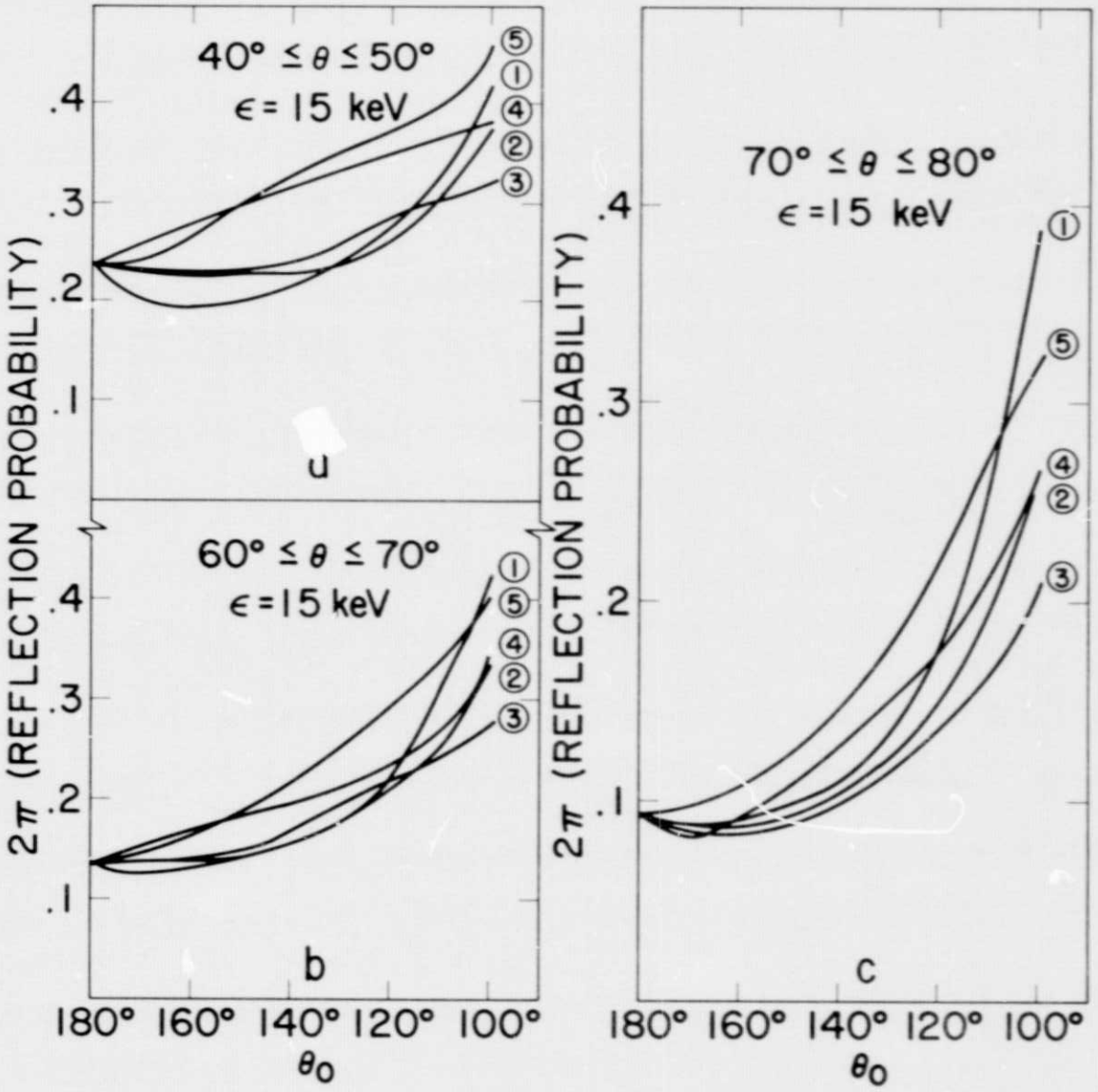
40° ≤ θ ≤ 50°
ϵ = 15 keV
a
60° ≤ θ ≤ 70°
ϵ = 15 keV
b
70° ≤ θ ≤ 80°
ϵ = 15 keV
c
2π (REFLECTION PROBABILITY)
.1
.2
.3
.4
①
②
③
④
⑤
180° 160° 140° 120° 100°
θ0

Fig. 8

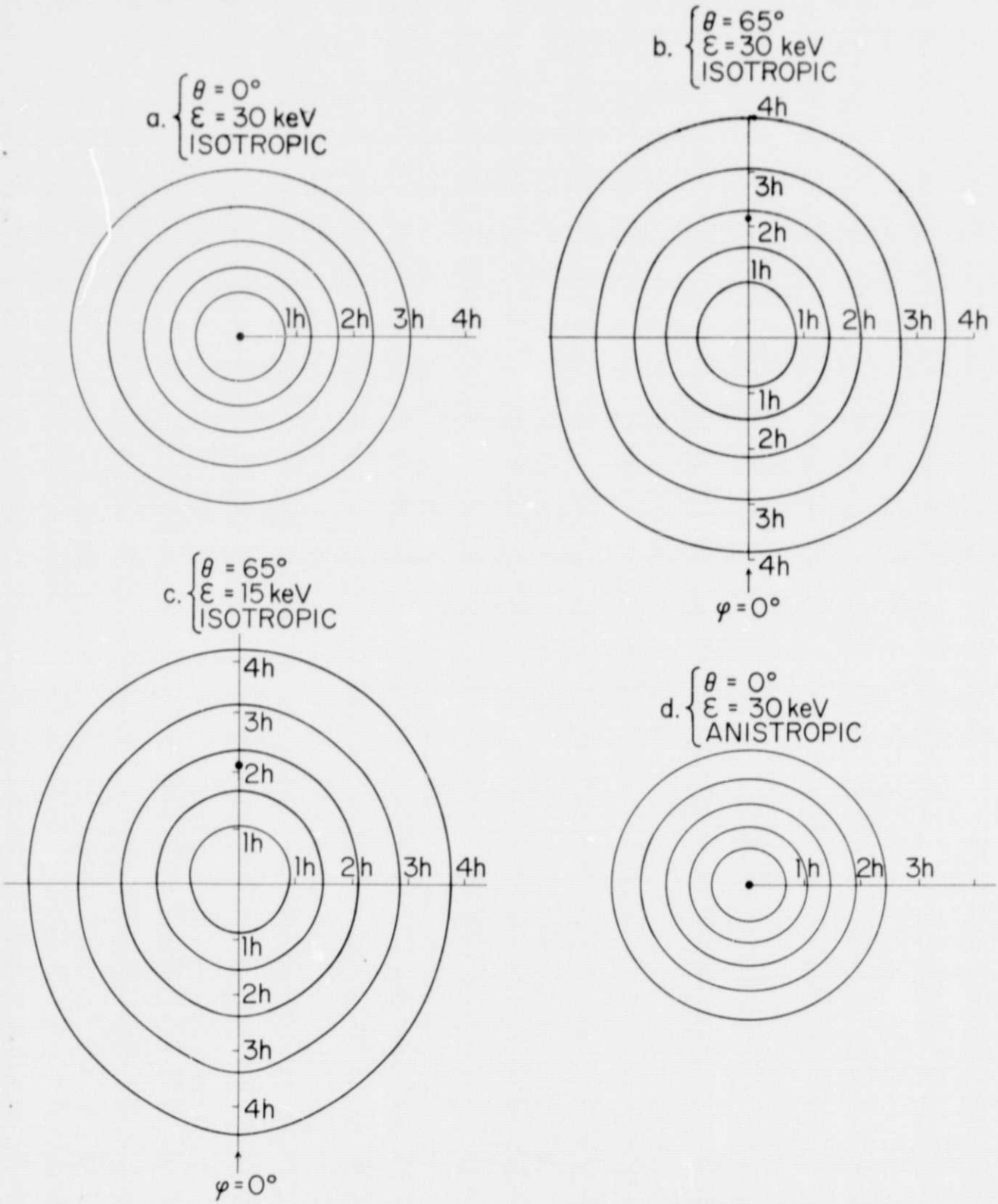
a. θ = 0°
Ɛ = 30 keV
ISOTROPIC
1h
2h
3h
4h
b. θ = 65°
Ɛ = 30 keV
ISOTROPIC
4h
3h
2h
1h
1h
2h
3h
4h
1h
2h
3h
4h
φ = 0°
c. θ = 65°
Ɛ = 15 keV
ISOTROPIC
4h
3h
2h
1h
1h
2h
3h
4h
1h
2h
3h
4h
φ = 0°
d. θ = 0°
Ɛ = 30 keV
ANISTROPIC
1h
2h
3h

Fig. 9